Polymer Bulletin (2020) 77:2183–2203
https://doi.org/10.1007/s00289-019-02855-3

ORIGINAL PAPER

Novel catechol-derived phosphorus-based precursors for coating applications

Megh Patel[1] · Siddhesh Mestry[1] · Ganesh Phalak[1] · Shashank Mhaske[1]

Received: 5 December 2018 / Revised: 30 April 2019 / Accepted: 19 June 2019 / Published online: 21 June 2019

Abstract

Depletion of the petroleum resources and poor flame-retardant properties of the epoxy resins drive researchers to develop an epoxy resin with good heat stability from bio-resources. In the current research work, we have reported the synthesis of a novel crosslinking agent for epoxy from the catechol as a bio-resource which can be further modified to form epoxy resin as well. The synthesis of the flame-retardant epoxy resin (TOMPP) was performed in two separate steps which include the reaction of the catechol with phosphoryl chloride followed by the reaction of the remaining hydroxyl groups with the epichlorohydrin. The structures of the synthesized products were confirmed using Fourier transform infrared spectroscopy, nuclear magnetic resonance spectroscopy and hydroxyl and epoxy values. The thermogravimetric analysis and differential scanning calorimetry were performed to analyse the thermal stability of the cured films which showed thermal degradation temperatures of both TOMPP and THPP formulations were decreased as the concentration of the TOMPP and THPP increased, while glass transition temperature (T_g) values increased. The char yield value of the THPP formulations was increased with increasing concentration of the intermediate, but for TOMPP it decreased. 40% THPP showed the least current density in electrochemical impedance spectroscopy suggesting the good corrosion resistance property. Mechanical properties were found to be similar for both THPP and TOMPP formulations. Flame retardancy was checked by LOI and UL-94 tests which revealed 40% THPP formulation had the maximum LOI as 28 and self-extinguishing behaviour.

✉ Shashank Mhaske
stmhaske@gmail.com

Megh Patel
mvp.patel159@gmail.com

Siddhesh Mestry
siddhesh17mestry@gmail.com

Ganesh Phalak
ganeshphalak1391@gmail.com

[1] Department of Polymer and Surface Engineering, Institute of Chemical Technology, Mumbai, India

Graphic abstract

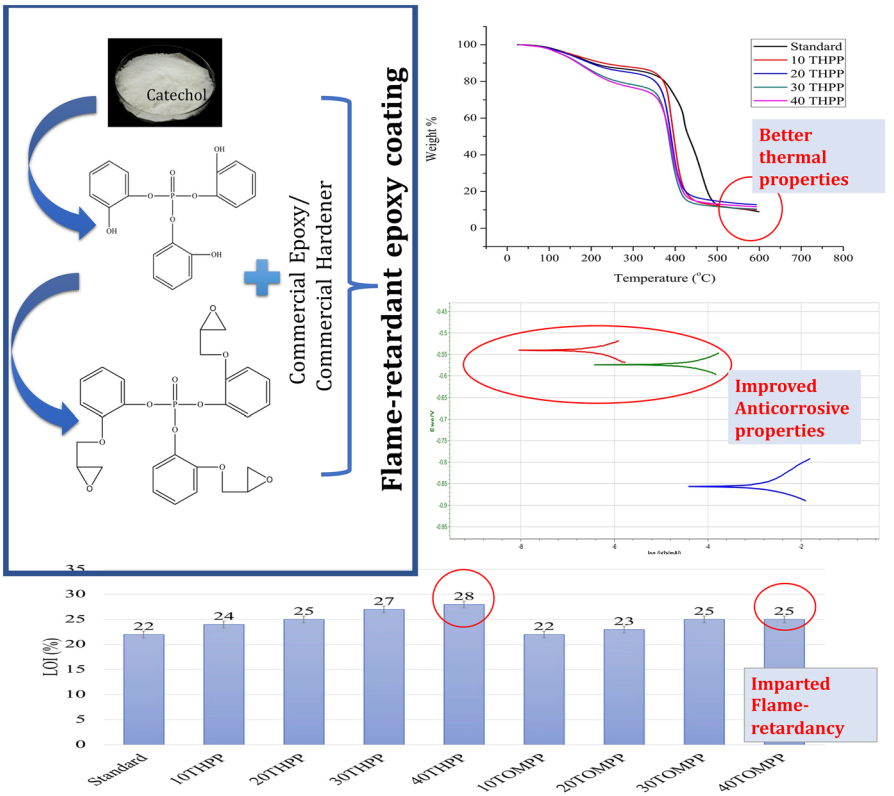

Keywords Catechol · Flame-retardant · Epoxy · Bio-based · Crosslinker

Introduction

Epoxy resins have been used immensely in diverse applications like construction, surface coatings, automotive, adhesives, laminates and insulating materials because of their excellent mechanical properties, good insulation property, thermal stability, moisture and chemical resistance, good barrier properties and very low shrinkage upon curing [1–4]. However, being an assortment of such superlative properties, epoxy resins lack the flame-retardant property [5]. Hence, this is becoming the main concern of the epoxy world and prompting researchers to introduce flame retardancy into the epoxy resins [6, 7]. Flame retardancy can be introduced by just physical mixing of the additive-type flame retardants into the polymer matrix or by chemical bonding to the polymer backbone. Additive type of flame retardants tends to leach out over the time; hence, they are quite discontinued. Also, halogen-containing

compounds release toxic and corrosive gases which are hazardous to human health and the environment [8]. As a result, phosphorous-, sulphur- and nitrogen-containing compounds got considerable attention to design flame-retardant resins. Phosphorus compounds act through forming a char layer between the substrate and the flame in which they combust to produce polymeric char layer and water which enhances the flame-retardant effect by cooling [9]. The synergistic effects of nitrogen and sulphur were reported to get the desired mechanical and adhesion properties of the epoxy coatings [9–12]. The multifunctional phosphorus-containing compounds for the curing of the epoxy coatings have been synthesized and used earlier for the better mechanical, thermal and flame-retardant properties [13–17].

Use of biomass resources to synthesize polymers can help to develop low-cost and environment-friendly products. There are many reports on the synthesis of epoxy resins from bio-resources like cardanol, vanillin, gallic acid, citric acid, isosorbide, lignin, etc. Catechol, the ortho isomer of the three benzenediols, is one of the bio-resource which is extracted from the concentrated juice of *Mimosa catechu* [18]. Nowadays, catechol is studied for the many applications in polymer industries such as anti-corrosive coatings, composites and UV-curable coatings [19–22].

The current study presents an attempt to develop a flame-retardant coating from catechol as a bio-resource. The precursor was made by the reaction of catechol and the phosphorus oxychloride which was used as a crosslinker along with the commercial epoxy: hardener system. The product of the first step was modified further with epichlorohydrin to develop an epoxy coating. This epoxy was also then used in various ratios along with the commercial epoxy: hardener system. The structure confirmation of the products was done using hydroxyl and epoxy values and supported by Fourier transform infrared (FTIR) spectroscopy and nuclear magnetic resonance (NMR) spectroscopy. Various mechanical and thermal properties of the cured coating films were checked and presented here along with the flame-retardant and anti-corrosive properties.

Materials and methods

Materials

Catechol, triethylamine (TEA), phosphorus oxychloride ($POCl_3$), epichlorohydrin (ECH), tetra-butyl ammonium bromide (TBAB), sodium hydroxide (NaOH), calcium oxide (CaO) and ethyl acetate (EA) were procured from S D Fine Chemicals Ltd., India. All the chemicals were used as produced without any treatment. Epoxy resin obtained from Grand Polycoats Co. Pvt. Ltd., Vadodara, was used as the source of commercial epoxy, while polyetheramine D230 from BASF Ltd. was used as a commercial hardener. The mild steel panels were used as a substrate for the coatings.

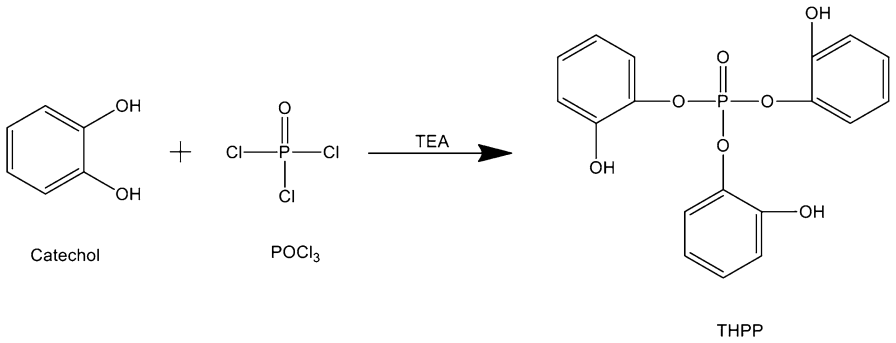

Scheme 1 Synthesis of THPP

Reaction of catechol and $POCl_3$

In a 250-mL three-necked round-bottom flask equipped with a mechanical stirrer, dropping funnel and nitrogen supply into the ice bath catechol (20.98 g, 0.19 mol) was charged along with EA as a solvent (40 mL) and TEA (19.28 g, 0.19 mol) as a catalyst. Phosphorus oxychloride (9.73 g, 0.063 mol) was then added dropwise under N_2 atmosphere by maintaining the temperature below 5 °C using an ice bath. After addition, the reaction mass was stirred continuously for 24 h at 50 °C. The reaction mass was then filtered to remove salts to get tris(2-hydroxyphenyl) phosphate (THPP) (Scheme 1).

Reaction of THPP and ECH

THPP (7.48 g, 0.02 mol) and ECH (27.2 g, 0.29 mol) were charged in a three-necked round-bottom flask equipped with a condenser and a mechanical stirrer along with TBAB (0.05 wt%) as a phase transfer catalyst. The obtained reaction mixture was stirred for 3 h at 115 °C. Then, the temperature was dropped down to 60 °C and NaOH (2.4 g, 0.06 mol) and CaO (0.1 wt%) were added as a catalyst and as a desiccant, respectively. The reaction was continued to stir for 4 h followed by the filtration and removal of excess ECH under vacuum to obtain light yellow-coloured tris(2-(oxiran-2-ylmethoxy) phenyl) phosphate (TOMPP) as a product (Scheme 2).

Preparation of the coating samples

The coatings were prepared by direct mixing of the obtained compounds in the required ratios along with the commercial epoxy: hardener system. In the case of THPP formulations, commercial hardener was partially replaced with the corresponding amount of THPP, while in TOMPP formulations, the commercial epoxy resin was partially replaced by TOMPP. The detailed formulations are given in Table 1. The obtained formulations were applied on the steel panels and cured in an oven at 120 °C for 4 h after air drying of 1 h. The steel panels were rubbed using sandpaper and cleaned with acetone prior use.

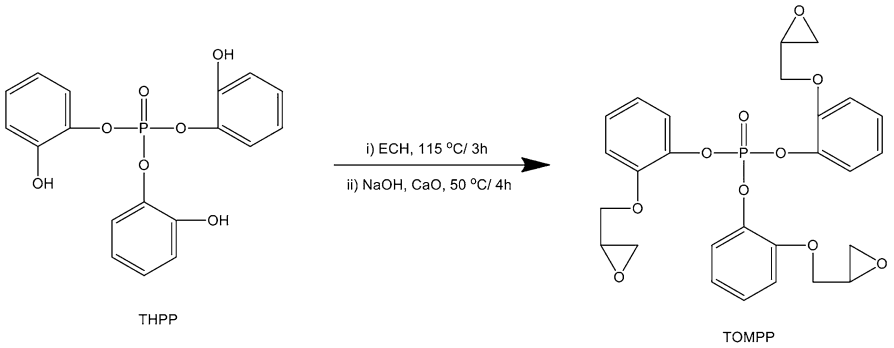

Scheme 2 Synthesis of TOMPP

Table 1 Formulations of the coating samples

Sample	Commercial epoxy (g)	Jeffamine (g)	THPP/ TOMPP (g)
Standard	1	0.62	0.0
10 THPP	1	0.56	0.2
20 THPP	1	0.50	0.4
30 THPP	1	0.44	0.6
40 THPP	1	0.38	0.8
10 TOMPP	1.8	1.189	0.2
20 TOMPP	1.6	1.128	0.4
30 TOMPP	1.4	1.067	0.6
40 TOMPP	1.2	1.006	0.8

Techniques and analyses

To evaluate the hydroxyl groups present on THPP, hydroxyl value was calculated according to ASTM D4272-16 using the acetic anhydride–pyridine method. The hydroxyl value was calculated using the following equation:

$$\text{Hydroxyl value} = \frac{[B - S] \times N \times 56.1}{W} \tag{1}$$

where B burette reading for blank (mL), S burette reading for sample (mL), N normality of alcoholic KOH solution, and W weight of sample (g).

Similarly, the epoxy equivalent weight (EEW) of TOMPP was calculated according to ASTM D-1652 by using the equation mentioned below:

$$\text{EEW} = \frac{W_s \times 1000}{[B - S] \times N} \tag{2}$$

where B burette reading for blank (mL), S burette reading for sample (mL), N normality of alcoholic KOH solution, and Ws weight of sample (g).

To determine the gel content, the cured films were carefully peeled off from the Teflon sheet. The known weight of polymer film was kept in the solvent mixture (50:50) of xylene and dimethylformamide (DMF) at room temperature for 24 h followed by the drying of the film at 80 °C until a constant weight was achieved. The gel content of the cured film was then determined by the formula:

$$\text{Gel content (\%)} = \frac{\text{Initial weight of the coating}}{\text{Weight of the coating after 24 h of solvent immersion}} \times 100 \tag{3}$$

ASTM D570 was used to determine the water absorption of the cured coating film in which the film was weighed before soaking into the water for 24 h. After 24 h, the film was removed from the water and dried with a paper towel to achieve a constant weight. Water absorption was determined from the differences in the weight of samples before and after soaking in the water according to the following equation:

$$\text{Water absorption (\%)} = \frac{\left(W_f - W_i\right)}{W_i} \times 100 \tag{4}$$

where W_f final weight of the coating after water absorption test and W_i initial weight of the coating before water absorption test.

The chemical structures of THPP and TOMPP were identified by Fourier transform infrared (FTIR) spectroscopy on a Bruker ATR spectrophotometer, USA. The spectra were observed in the 600–4000 cm^{-1} wavelength range. The structure confirmation of THPP and TOMPP was done by ^{1}H and ^{13}C nuclear magnetic resonance (NMR) spectroscopy. ^{1}H and ^{13}C NMR spectra of the product were analysed using Bruker DPX 800 MHz spectrophotometer with dimethyl sulphoxide (DMSO) as a solvent.

Thermogravimetric analysis (TGA) of cured epoxy films was conducted on Perkin-Elmer TGA 4000 instrument under the nitrogen atmosphere. Thermal analysis was performed in the temperature range of 40–600 °C with 20 °C/min heating rate. Differential scanning calorimetry (DSC) (TA Q100 analyser, USA) was employed for the determination of the glass transition temperature (T_g) of cured films. The film sample weighed accurately in an aluminium pan and heated in 40–120 °C temperature range with the heating rate of 10 °C/min.

Electrochemical impedance spectroscopy (EIS) was performed using SP-300-Potentiostat driven by EC-Lab software by sweeping the potential from equilibrium potential towards negative and positive potentials against platinum reference electrode in 3.5% (w/w) NaCl electrolyte with 10 mV peak to peak perturbation within the frequency range of 100 mHz–10 kH. The test was carried out once the OCP (open-circuit potential) had been reached. Corrosion performance was calculated using the slope of Tafel plot, and an increase/decrease in current density with respect to overpotential was observed. The observations were potentiodynamic, and linear polarization was used to plot the Tafel plot.

The coatings were characterized by performing various mechanical tests according to ASTM standards. The adhesion of the coating to the substrate was examined

by the cross-cut test according to ASTM D-3359. On the coating surface, lattice marking of 1 cm^2 was done until the metal surface was exposed followed by the application of adhesion tape over lattice marking. The adhesive tape was then pulled out from the coating surface, and adhesion failure was examined over the lattice marking as per ASTM standard. Pencil hardness test was carried out according to the ASTM D-3363. Scratch was made on the coating surface by using 6B–6H range of pencils at an angle of 45°. Impact properties of the coatings were evaluated by dropping a weighted ball of 1.36 kg from the maximum height of 60 cm onto the coated surface. The flexibility of the coatings was evaluated by using conical mandrel as per ASTM D-522. The coated panels were fixed onto a conical mandrel and were bent to analyse the coating flexibility.

The flammability of the cured samples was investigated by limiting oxygen index (LOI) test carried out on Dynisco, USA, according to ASTM D2863 procedure. The UL-94 vertical burning test was carried out according to ASTM D1356-2005. Sample specimens having a size of $125 \times 12.5 \times 3$ mm were mounted vertically, and the flame was introduced for 10 s to the specimen at an angle of 45°. The detailed rating is given in Table 2.

Results and discussion

Physicochemical analysis

The physicochemical analysis was done to evaluate the structure of both compounds using equivalents of the functional group present in the molecule. The theoretical and practical values obtained after the calculations were comparable suggesting the desired compound formation. The details are given in Table 3.

Table 2 UL-94 rating

Rating	Description
V-0	Burning stops within 10 s on a vertical specimen; drips of particles allowed as long as they are not inflamed
V-1	Burning stops within 30 s on a vertical specimen; drips of particles allowed as long as they are not inflamed
V-2	Burning stops within 30 s on a vertical specimen; drips of flaming particles are allowed

Table 3 Physicochemical analysis of THPP and TOMPP

Sample	Hydroxyl value (mg KOH/gm)		Epoxy equivalent weight (gm/equivalent)	
	Theoretical	Practical	Theoretical	Practical
THPP	407.32	402.05	–	–
TOMPP	–	–	180.82	176.54

FTIR and NMR analyses

FTIR was done to evaluate the completion of the reaction and the desired product formation. The samples were used in their original state, i.e. liquid without any chemical or heat treatment. FTIR spectrum of the catechol is shown in Fig. 1 and the spectra of THPP and TOMPP are illustrated in Fig. 2, while the important characteristic absorption bands are given in Table 4.

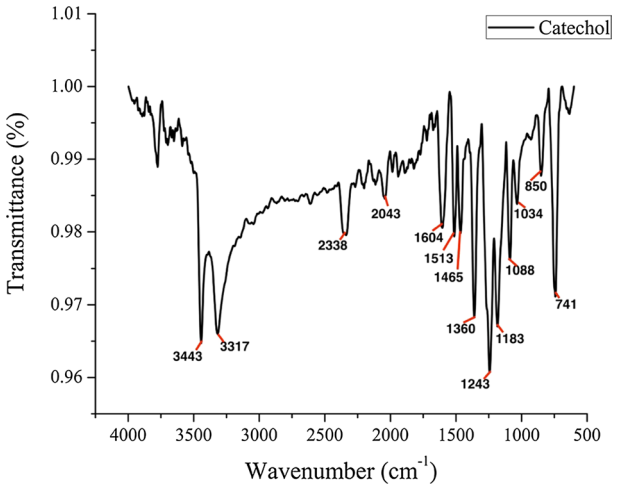

Fig. 1 FTIR spectrum of catechol

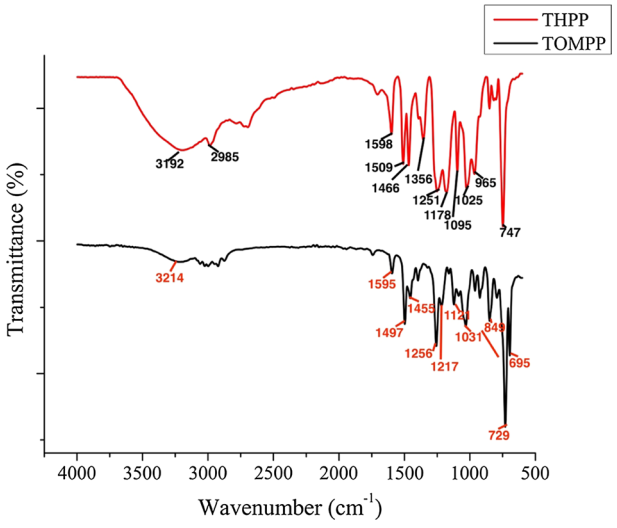

Fig. 2 FTIR spectra THPP and TOMPP

Table 4 FTIR characteristic absorption peaks

Functionality	Catechol	THPP	TOMPP
–OH stretch	3443 cm^{-1}, 3317 cm^{-1}	3192 cm^{-1} (plateau)	3214 cm^{-1} (almost disappeared)
C=C ring	1604 cm^{-1}	1598 cm^{-1}	1595 cm^{-1}
C–O and –OH	1360 cm^{-1}	1356 cm^{-1} (intensity lowered)	Disappeared
C–C	741 cm^{-1}	747 cm^{-1}	729 cm^{-1}
P–O–C	–	1025 cm^{-1}	1031 cm^{-1}
P=O	–	1095 cm^{-1}	1121 cm^{-1}
Oxirane	–	–	849 cm^{-1}

According to Fig. 1, the presence of –OH in the catechol is shown by the peaks at 3443 cm^{-1} and 3317 cm^{-1}. The peaks at 1604 cm^{-1} and 1513 cm^{-1} are attributed to C=C stretching vibrations present in the aromatic ring of catechol. The peaks at 1360 cm^{-1}, 1243 cm^{-1} and 1183 cm^{-1} show the C–O and O–H stretching vibrations due to phenolic –OH in the catechol, while the peaks at 1088 cm^{-1} and 1034 cm^{-1} show the presence of C–O stretching and C–H deformation vibrations. The sharp peak at 741 cm^{-1} is due to C–C vibrations.

Figure 2 compares the important changes in the FTIR spectra of THPP and TOMPP. As seen from Fig. 1, O–H and C–O stretching vibration peaks appeared in the range of 3317 cm^{-1}–3443 cm^{-1} and 1360 cm^{-1}–1183 cm^{-1} whose intensity seems to be lowered in the FTIR spectrum of THPP and transforming into a plateau region at 3192 cm^{-1} suggesting the partial consumption of the hydroxyl groups. The newly formed peaks at the 1025 cm^{-1} and 965 $cm^{-}1$ are attributed to the formation of P–O–C linkages in the molecule, while the peak at 1095 cm^{-1} shows the presence of P=O stretching vibration.

The disappearance of O–H stretch in the FTIR spectrum of TOMPP demonstrates the reaction of the remaining hydroxyls with ECH. The next important characteristic peak that comes into sight is the peak at 849 cm^{-1} which indicates the presence of oxirane ring in the molecule [23].

The structures obtained were further confirmed by NMR analysis. The ^{1}H-NMR and ^{13}C-NMR spectra of THPP and TOMPP are shown in Figs. 3a to 4b, respectively. ^{1}H-NMR spectrum of THPP shows all the characteristic peaks of hydroxyls present in the catechol in the plateau region of 4 -4.5 ppm. All the peaks corresponding to the protons of the aromatic rings in the molecule have appeared in 6.3–7.1 ppm. Similarly, ^{13}C-NMR spectrum of THPP shows the characteristic peaks in 115–125 ppm and 145–165 ppm. Figure 4a shows ^{1}H-NMR spectrum of TOMPP epoxy resin which shows the characteristic peaks of the presence of ECH in the region of 2.5–3.8 ppm, while ^{13}C-NMR spectrum shows the presence of ECH around 46, 52 and 70 ppm.

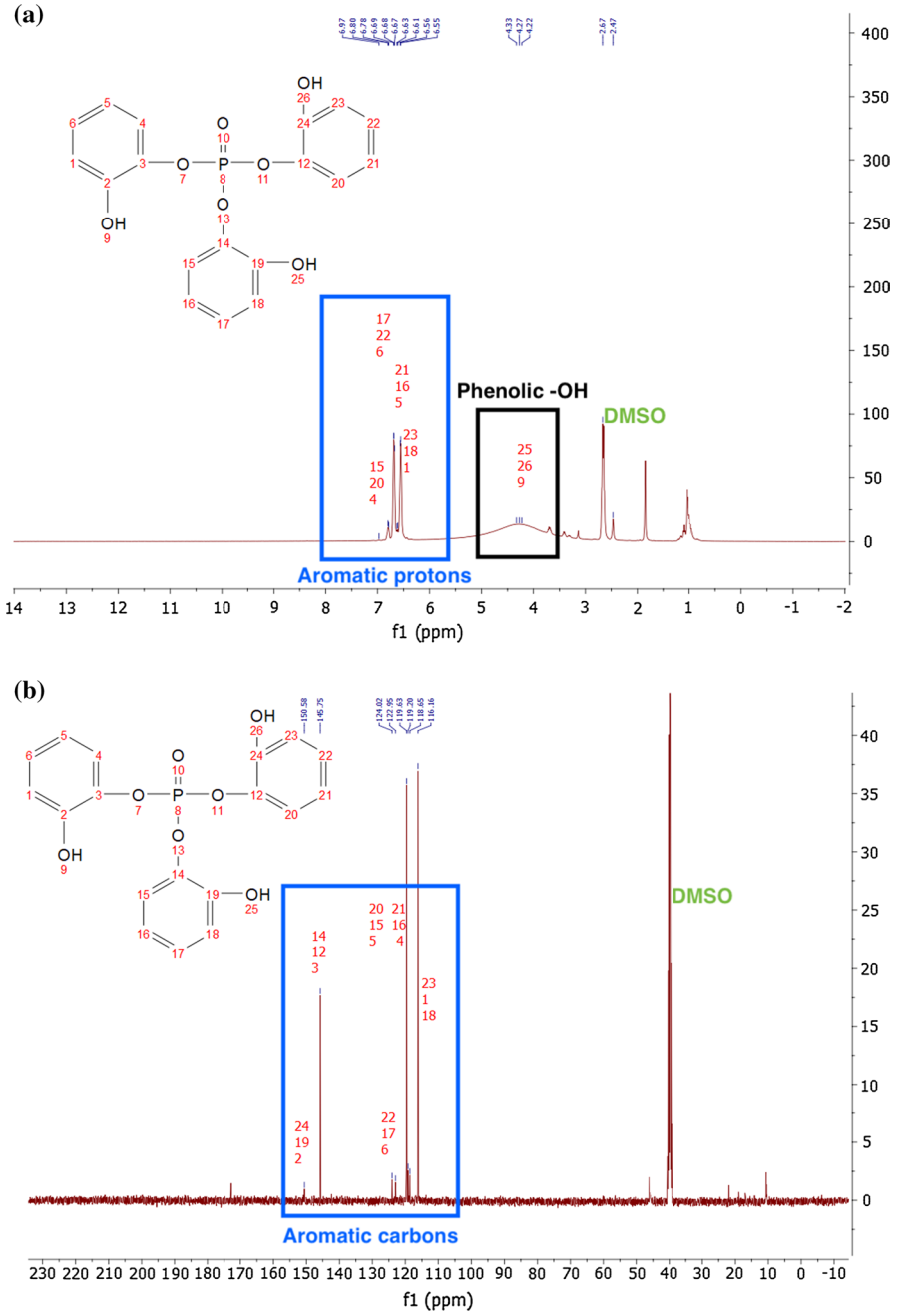

Fig. 3 **a** ^{1}H-NMR spectrum of THPP. **b** ^{13}C-NMR spectrum of THPP

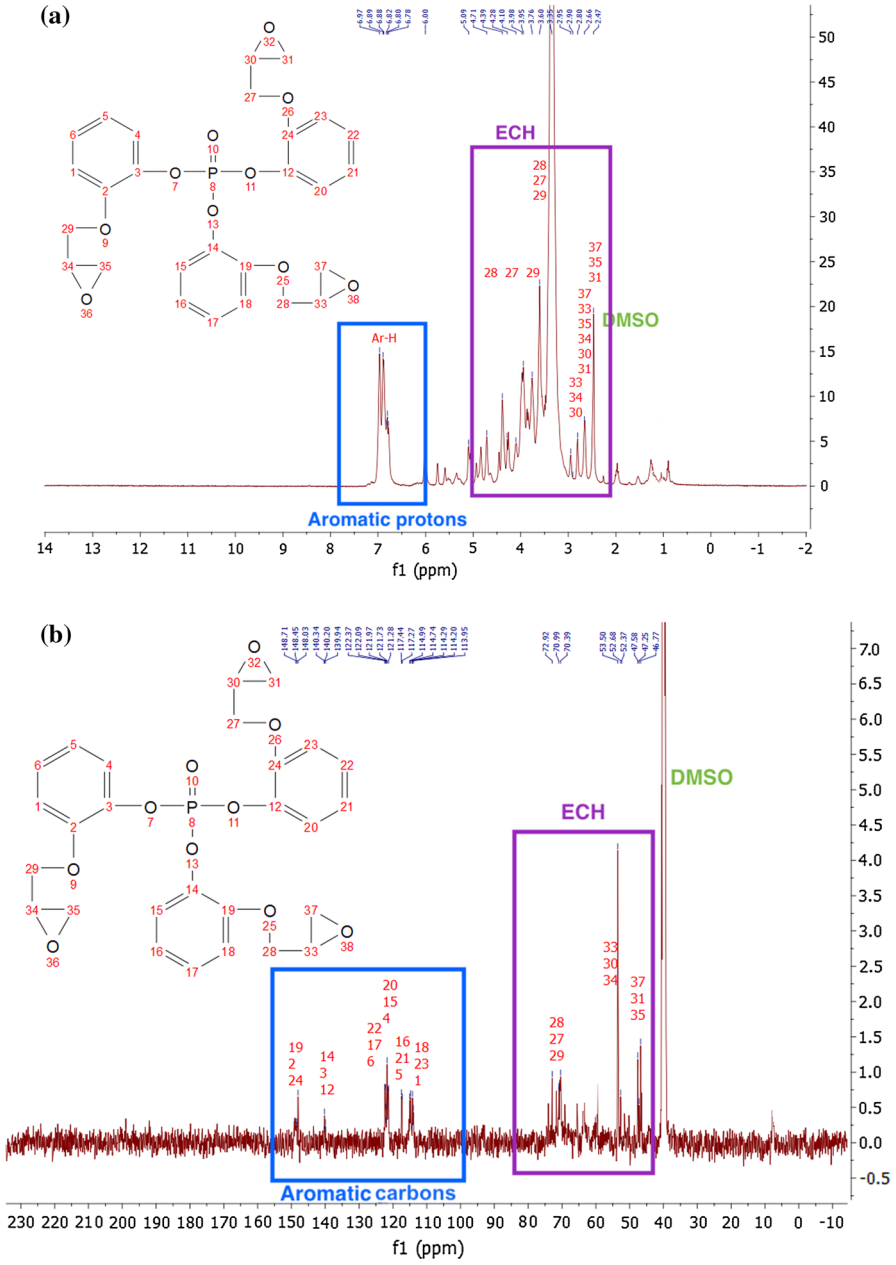

Fig. 4 **a** ^{1}H-NMR spectrum of TOMPP. **b** ^{13}C-NMR spectrum of TOMPP

Thermal properties

The changes in the physical and chemical properties of the cured samples as a function of increasing temperature against a weight loss were studied using TGA. The comparison of TGA plots of THPP and TOMPP formulations is shown in Fig. 5a, b, respectively, while the thermal characteristic values are given in Table 5. The results reveal that as the phosphorus content in the backbone increases, the thermal stability of the THPP formulations increases while the negative effect on the TOMPP formulations. The initial degradation temperatures of both the formulations had decreased except for the 10% loading of the phosphorus-containing moiety. 10% loaded formulations had showed the optimum results in case of initial thermal stability of the material which deteriorated as the loading increased further. Ideally, phosphorus

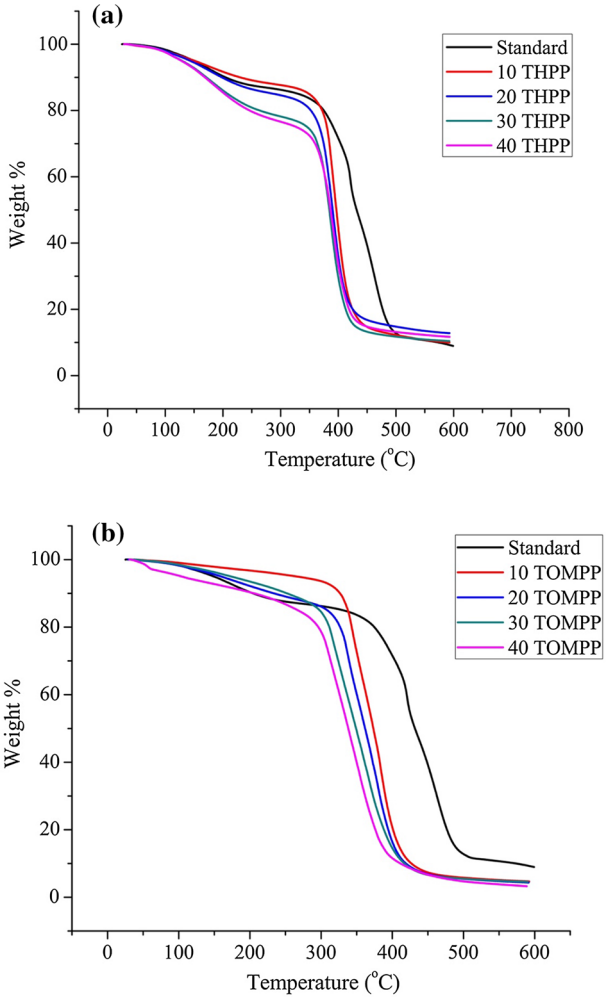

Fig. 5 **a** TGA curves of THPP formulations. **b** TGA curves of TOMPP formulations

Table 5 Thermal characteristic behaviour of THPP and TOMPP formulations

Sample	15% Weight loss (°C)	30% Weight loss (°C)	Char yield at 600 °C (%)	T_g (°C)
Standard	328.1	392.7	8.9	121.6
10 THPP	349.26	384.50	9.98	135.77
20 THPP	289.11	374.57	12.80	140.08
30 THPP	208.17	363.55	10.43	145.10
40 THPP	202.81	359.76	11.68	145.18
10 TOMPP	337.5	352.6	4.6	126.78
20 TOMPP	308.6	339.3	4.3	139.56
30 TOMPP	298.0	323.9	4.5	144.52
40 TOMPP	267.3	312.8	3.2	145.24

would have increased the thermal stability with the increasing concentration, but one may have to think of the other factors which might affect the overall thermal stability of the material [8, 24]. Owing to bulky nature of the chemical structures of the synthesized THPP and TOMPP, there has to be some amount of steric hindrance present due to three benzene rings and at the same time, these structures being multifunctional act as a crosslinking builder in the coating system. Hence, though the thermal stability should increase because of the phosphorus, there are some adverse effects present because of the chemical structure of the synthesized molecules [25, 26].

As seen from the results, the char yield values also increased up to a certain amount of loading of the THPP or TOMPP. 20 THPP had the maximum amount of char yield as 12.8%, while 10 TOMPP had the maximum char yield value in TOMPP formulations as 4.68%. TOMPP formulations showed lower char yields may be because of increased voids in the polymer network because of the bulky structure which led to a decrease in the thermal stability of the resin. Also, the degradation characteristics showed a decrease in the initial as well as final degradation temperatures beyond the loading of the optimum formulation. The probable reasons for the same are the crosslinking density and the bulkiness of the THPP and TOMPP. As the crosslinking density had increased in some areas due to multifunctionality, the stacking of the polymer chains over one another was prevented by the bulky structure of the molecules simultaneously [24, 27]. TOMPP formulations showed the lower values of degradation temperatures as well as of char yields than THPP formulations, which might be explained by the further increase in the bulkiness of the molecule by addition of ECH which is increasing the intermolecular distance and could have prevented the proper stacking of the polymer chains resulting in the more voids and further deteriorating thermal properties.

The results of DSC analysis are shown in Fig. 6a, b which determine the temperature and heat flow associated with material transitions as a function of time and temperature. The results of DSC show that for both the THPP and TOMPP formulations, T_g values have increased with increase in the concentration of the phosphorus-containing moiety. This can be explained by the increasing crosslinking density, brittleness and the rigidity due to the benzene ring present in the molecules [28, 29]. The fact of increasing voids in the system due to bulky structures of THPP and

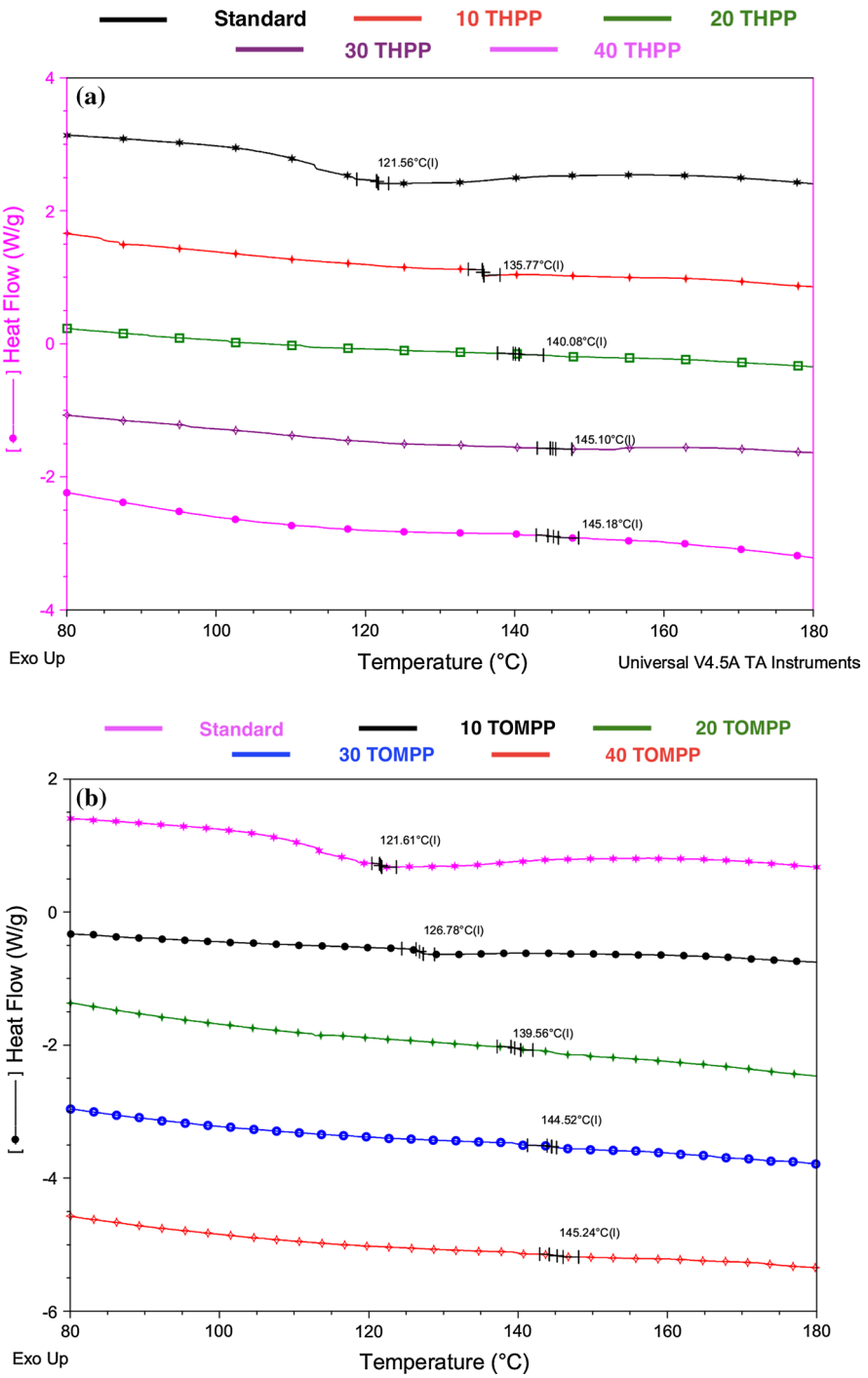

Fig. 6 **a** DSC flow charts of THPP formulations. **b** DSC flow charts of TOMPP formulations

Table 6 Mechanical properties of the THPP and TOMPP formulations

Sample	Impact test	Flexibility	Pencil hardness	MEK test	Cross-hatch test
Standard	60	Pass	6H	> 450	Pass
10 THPP	60	Pass	6H	> 450	Pass
20 THPP	60	Pass	6H	> 400	Pass
30 THPP	40	Fail	4H	> 315	Fail
40 THPP	30	Fail	H	> 300	Fail
10 TOMPP	60	Pass	6H	> 450	Pass
20 TOMPP	50	Fail	4H	> 400	Fail
30 TOMPP	30	Fail	3H	> 310	Fail
40 TOMPP	20	Fail	B	> 280	Fail

TOMPP could have caused the coatings to have low T_g values because of improper stacking of the polymer chains, but the rigidity of both the molecules and the crosslinking density might be governing the T_g values to the higher side.

Mechanical properties

Various tests such as impact, flexibility, pencil hardness, cross-hatch test were performed on the coated panels to evaluate the mechanical properties of the coatings. Generally, the changes in the crosslinking density obtained by the modification in the resin govern the mechanical properties, gel content and the water absorption of the coatings [30]. Excellent mechanical properties were attributed to the strong crosslink network obtained with three-arm structures of THPP and TOMPP up to certain loading, but the properties were similar to the standard for higher concentrations of the synthesized products. As discussed in the previous sections, these results also can be related to the brittleness of the films due to the bulky structures of THPP and TOMPP. There was no crack observed in the impact tests even from the 60-cm fall of the ball for 30% loading of THPP and 20% loading of TOMPP but after these concentrations films were found to be more brittle. Similar kind of results was observed in the case of flexibility and pencil hardness tests. The cross-hatch test reflected the results as expected from the other mechanical properties testing; due to brittle films, the formulations with higher concentrations of THPP and TOMPP showed low adhesion to the mild steel substrate. The solvent scrub resistance is dependent partially on the adhesion of the coating to the substrate while partially on the resistance to the solvent which led to lower resistance of the 30 THPP, 40 THPP, 20 TOMPP, 30 TOMPP and 40 TOMPP to the MEK scrub test. For TOMPP formulations, we can see from the T_g values that only the T_g has increased due to the increased rigidity of the overall system, but at the same time voids in the matrix have increased which led to the deterioration of the mechanical properties. The gel content and water absorption were controlled by the crosslinking density and the nature of the coating which showed peak gel content value for 20 THPP and 10 TOMPP and thus the lowest water absorption. The obtained results are depicted in Table 6 and Fig. 7.

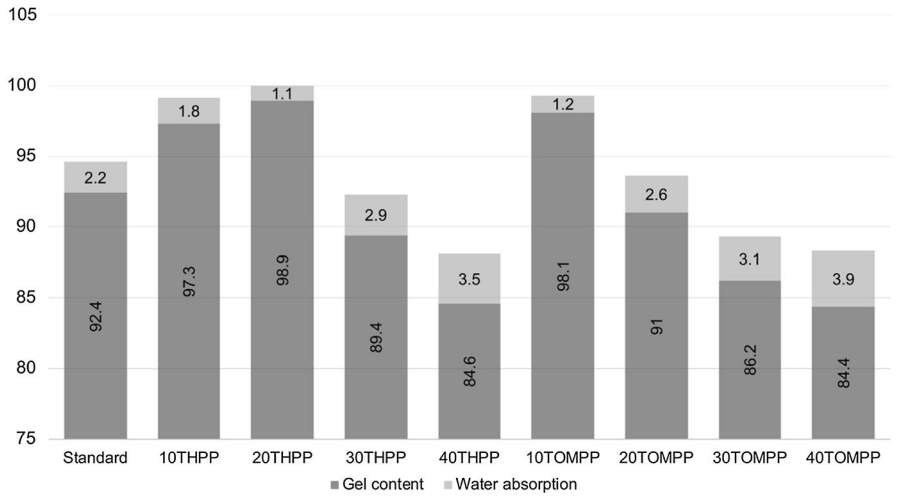

Fig. 7 Gel content and water absorption of THPP and TOMPP formulations

EIS results

The logical method to evaluate the corrosion protection abilities of the coating material for mild steel is the Tafel plot. In a typical Tafel polarization curve, the excellent corrosion resistance of the coating is shown by the lower corrosion rate (C_R), which corresponds to a higher corrosion potential (E_{corr}) or a lower corrosion current density (I_{corr}) [31–33]. Two of the best formulations in terms of the other properties obtained were selected from the series of THPP and TOMPP as 20 THPP and 10 TOMPP for the corrosion resistance analysis and tested against the standard epoxy coating. Figure 8 shows the Tafel plots of the standard and THPP- and TOMPP-coated samples, and the corrosion data obtained from the anodic and cathodic curves are given in Table 7. The C_R values of the samples were calculated from the following Eq. (5):

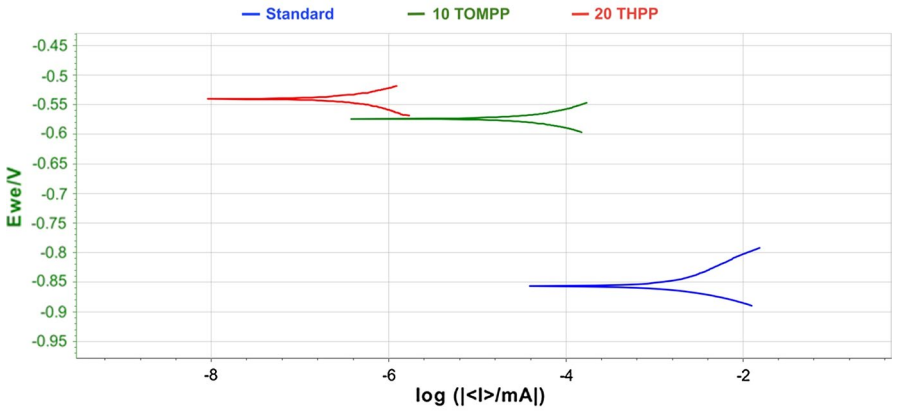

Fig. 8 Tafel plots of the standard, THPP and TOMPP epoxy formulations

Table 7 Corrosion properties of the coated epoxy formulations

Sample	E_{corr} (mV)	I_{corr} (μA)	C_R (mpy)	%PE
Standard	− 838.2	7.58	3.58	–
10 TOMPP	− 574.5	0.04	0.0189	99.47
20 THPP	− 537.4	0.00036	0.00865	99.99

$$C_R = 3270 \times \frac{M(g) \times I_{corr}\left(\frac{A}{cm^2}\right)}{n \times \rho\left(\frac{g}{cm^3}\right)} \tag{5}$$

where M is the molecular weight of steel, I_{corr} is determined from Tafel plots, n is the valence (the number of electrons lost during the oxidation reaction), ρ is the density of steel, and 3270 represents the unit of corrosion rate. It can be found from the corrosion data that the incorporation of the synthesized compounds has lowered the corrosion rate of the commercial epoxy coating.

The reasons for the same can be explained by the mechanism of blocking pinholes and passivation of the surface due to blocking caused by the loading of THPP or TOMPP while evaporation of the solvents. This formation of the passive film layer would prevent the permeation of a corrosive medium leading to building up the anti-corrosive property. THPP formulation had the highest anti-corrosion ability due to the proper crosslinking and the increased barrier properties as seen from the results of the gel content and water absorption. TOMPP formulation showed slightly less corrosion protection efficiency which can be attributed to the structure of the TOMPP molecule that led to an increase in voids of the formed coating matrix [34, 35]. The corrosion protection efficiency (PE) with respect to the standard was calculated using the following equation:

$$\%PE = \frac{I'_{corr} \times I_{corr}}{I'_{corr}} \times 100 \tag{6}$$

where I'_{corr} is the corrosion current of the standard epoxy coating, while I_{corr} is the corrosion current of THPP and TOMPP epoxy samples.

Flame-retardant properties

The flame-retardant properties of the various epoxy formulations were checked by LOI and UL-94 vertical burning tests. It was observed that the standard epoxy coating had the lowest LOI as compared to other THPP and TOMPP formulations. The highest LOI was shown by 40 THPP which can be supported by the DSC results and the char yield values of THPP formulations. The crosslinking density, the phosphorus and the rigid structure of the benzene ring had played a vital role in increasing

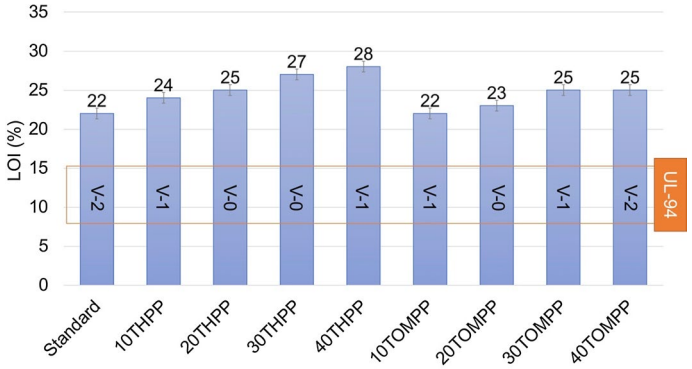

Fig. 9 LOI and UL-94 ratings of epoxy formulations

the flame retardancy of the overall system. TOMPP formulations did not show much increase in the LOI values which can be explained by discontinuous structure or the presence of voids due to bulky nature of TOMPP molecule that led to a decrease in the flame-retardant stability of the coating systems. UL-94 vertical burning test showed that standard, 10 THPP, 20 THPP, 10 TOMPP and 20 TOMPP showed the self-extinguishing behaviour within 10 s when the flame was removed with no dripping of the material while other formulations dripped while testing. 30 THPP, 40 THPP and 30 TOMPP could self-extinguish the fire within 40 s from burning. The self-extinguishing behaviour and dripping of the coatings can be related to the structural stability of the material while combustion. The samples which had the good thermal degradation temperatures and in particular high T_g showed good structural stability with the negligible amount of dripping or no dripping of the material. LOI values and UL-94 ratings of the various coating formulations are shown in Fig. 9.

Conclusion

The flame-retardant precursors for the partial replacement of the commercial epoxy resin as well as for commercial hardener were successfully synthesized from a bio-based material as catechol. The structure confirmations were done using the epoxy and hydroxyl values which were supported by the FTIR and NMR results. The flame retardancy was checked using LOI and UL-94 vertical burning test which showed that 40 THPP had the high LOI value and no dripping even at high concentration of THPP. THPP formulations had better structural stability due to the crosslinking density and the presence of rigid benzene ring and phosphorus reflected in the char yield, T_g and thermal degradation results. TOMPP formulations failed to have such good thermal characteristic properties which could be due to the increased bulky nature of the TOMPP molecule, thus deteriorating the barrier properties as well. A similar trend of results was observed in the gel content and water absorption tests where crosslinking density and packing of the polymer chains usually drive the properties. 20 THPP and 10 TOMPP were selected as the good formulations

among all depending upon the results obtained in other tests which were then tested for the corrosion resistance occurring due to the incorporation of the synthesized compounds. 20 THPP had the lowest corrosion rate and highest corrosion protection ability which could be attributed to the proper crosslinking and passivation of the surface due to blocking caused by the loading of THPP molecules in the system. THPP formed in first step can be used as a precursor for developing other types of resins like polyurethanes, alkyds, etc., depending upon the desired properties.

References

1. Wang X, Song L, Xing W et al (2011) A effective flame retardant for epoxy resins based on poly(DOPO substituted dihydroxyl phenyl pentaerythritol diphosphonate). Mater Chem Phys 125:536–541. https://doi.org/10.1016/j.matchemphys.2010.10.020
2. Jian R, Wang P, Duan W et al (2017) A facile method to flame-retard epoxy resin with maintained mechanical properties through a novel *P*/*N*/*S*-containing flame retardant of tautomerization. Mater Lett 204:77–80. https://doi.org/10.1016/j.matlet.2017.05.135
3. Gao LP, Wang DY, Wang YZ et al (2008) A flame-retardant epoxy resin based on a reactive phosphorus-containing monomer of DODPP and its thermal and flame-retardant properties. Polym Degrad Stab 93:1308–1315. https://doi.org/10.1016/j.polymdegradstab.2008.04.004
4. Liang WJ, Zhao B, Zhao PH et al (2017) Bisphenol-S bridged penta(anilino)cyclotriphosphazene and its application in epoxy resins: synthesis, thermal degradation, and flame retardancy. Polym Degrad Stab 135:140–151. https://doi.org/10.1016/j.polymdegradstab.2016.11.023
5. Xu Y, Wang J, Tan Y et al (2018) A novel and feasible approach for one-pack flame-retardant epoxy resin with long pot life and fast curing. Chem Eng J 337:30–39. https://doi.org/10.1016/j.cej.2017.12.086
6. Shao ZB, Zhang MX, Li Y et al (2018) A novel multi-functional polymeric curing agent: synthesis, characterization, and its epoxy resin with simultaneous excellent flame retardance and transparency. Chem Eng J 345:471–482. https://doi.org/10.1016/j.cej.2018.03.142
7. Jian R, Wang P, Xia L, Zheng X (2017) Effect of a novel *P*/*N*/*S*-containing reactive flame retardant on curing behavior, thermal and flame-retardant properties of epoxy resin. J Anal Appl Pyrolysis 127:360–368. https://doi.org/10.1016/j.jaap.2017.07.014
8. Sonnier R, Dumazert L, Livi S et al (2016) Flame retardancy of phosphorus-containing ionic liquid based epoxy networks. Polym Degrad Stab 134:186–193. https://doi.org/10.1016/j.polymdegradstab.2016.10.009
9. Wang P, Xia L, Jian R et al (2018) Flame-retarding epoxy resin with an efficient *P*/*N*/*S*-containing flame retardant: preparation, thermal stability, and flame retardance. Polym Degrad Stab 149:69–77. https://doi.org/10.1016/j.polymdegradstab.2018.01.026
10. Wang P, Yang F, Li L, Cai Z (2016) Flame retardancy and mechanical properties of epoxy thermosets modified with a novel DOPO-based oligomer. Polym Degrad Stab 129:156–167. https://doi.org/10.1016/j.polymdegradstab.2016.04.005
11. Liang WJ, Zhao B, Zhang CY et al (2017) Enhanced flame retardancy of DGEBA epoxy resin with a novel bisphenol-A bridged cyclotriphosphazene. Polym Degrad Stab 144:292–303. https://doi.org/10.1016/j.polymdegradstab.2017.08.027
12. Shen D, Xu YJ, Long JW et al (2017) Epoxy resin flame-retarded via a novel melamine-organophosphinic acid salt: thermal stability, flame retardance and pyrolysis behavior. J Anal Appl Pyrolysis 128:54–63. https://doi.org/10.1016/j.jaap.2017.10.025
13. Suresh S, Srivastava VC, Mishra IM (2012) Adsorption of catechol, resorcinol, hydroquinone, and their derivatives: a review. Int J Energy Environ Eng 3(32):1–19. https://doi.org/10.1186/2251-6832-3-32
14. Tan Y, Shao ZB, Chen XF et al (2015) Novel multifunctional organic–inorganic hybrid curing agent with high flame-retardant efficiency for epoxy resin. ACS Appl Mater Interfaces 7:17919–17928. https://doi.org/10.1021/acsami.5b04570

15. Jue C, Juan L, Wantai Y (2009) Curing behavior and thermal properties of trifunctional epoxy resin cured by 4,4′-diaminodiphenylmethane. J Appl Polym Sci 114:1976–1983. https://doi.org/10.1002/app.30630
16. Gan J, Goodson A (2003) Flame retardant phosphorus element-containing epoxy resin compositions. US Patent 6,645,631B2
17. Mestry S, Mhaske ST (2019) Synthesis of epoxy resins using phosphorus-based precursors for flame-retardant coating. J Coat Technol Res. https://doi.org/10.1007/s11998-018-00157-3
18. Suresh S, Srivastava VC, Mishra IM (2012) Adsorption of catechol, resorcinol, hydroquinone, and their derivatives: a review. Int J Energy Environ Eng. https://doi.org/10.1186/2251-6832-3-32
19. Wu J, Cai C, Zhou Z et al (2016) Low-cost mussel inspired poly(catechol/polyamine) coating with superior anti-corrosion capability on copper. J Colloid Interface Sci 463:214–221. https://doi.org/10.1016/j.jcis.2015.10.056
20. Sa R, Wei Z, Yan Y et al (2015) Catechol and epoxy functionalized ultrahigh molecular weight polyethylene (UHMWPE) fibers with improved surface activity and interfacial adhesion. Compos Sci Technol 113:54–62. https://doi.org/10.1016/j.compscitech.2015.03.017
21. Wang L, Shi Y, Chen S et al (2017) Highly efficient mussel-like inspired modification of aramid fibers by UV-accelerated catechol/polyamine deposition followed chemical grafting for high-performance polymer composites. Chem Eng J 314:583–593. https://doi.org/10.1016/j.cej.2016.12.015
22. Liu Y, Wang R, Zhu Y et al (2015) Photoelectrochemical sensing of catechol based on CdS-DNA-pristine graphene nanocomposite film. Sens Actuat B Chem 210:355–361. https://doi.org/10.1016/j.snb.2014.12.124
23. González MG, Cabanelas JC, Baselga J (1998) In-Tech applications of FTIR on epoxy resins-identification, monitoring the curing process, phase separation and water uptake, infrared spectroscopy—materials science, engineering and technology. IntechOpen Publisher, New York
24. Jeng RJ, Shau SM, Lin JJ et al (2002) Flame retardant epoxy polymers based on all phosphorus-containing components. Eur Polym J 38:683–693. https://doi.org/10.1016/S0014-3057(01)00246-4
25. Wang S, Xu C, Liu Y et al (2017) Vanillin-derived high-performance flame retardant epoxy resins: facile synthesis and properties. Macromolecules. https://doi.org/10.1021/acs.macromol.7b00097
26. Chen X, Jiao C (2008) Thermal degradation characteristics of a novel flame retardant coating using TG-IR technique. Polym Degrad Stab 93:2222–2225. https://doi.org/10.1016/j.polymdegradstab.2008.09.005
27. Quin L, Ye L, Xu G, Liu J (2011) The non-halogen flame retardant epoxy resin based on a novel compound with phosphaphenanthrene and cyclotriphosphazene double functional groups. Polym Degrad Stab 96:1118–1124. https://doi.org/10.1016/j.polymdegradstab.2011.03.001
28. Chuan S, Ying L, Yie S (2002) Epoxy resins possessing flame retardant elements from silicon incorporated epoxy compounds cured with phosphorus or nitrogen containing curing agents. Polymer (Guildf) 43:4277–4284. https://doi.org/10.1016/S0032-3861(02)00234-3
29. Lokhande G, Chambhare S, Jagtap R (2017) Synthesis and properties of phosphate-based diacrylate reactive diluent applied to UV-curable flame-retardant wood coating. J Coat Technol Res 14:255–266. https://doi.org/10.1007/s11998-016-9849-6
30. Choi J, Seo J, Khan S (2011) Effect of acrylic acid on the physical properties of UV-cured poly(urethane acrylate-co-acrylic acid) films for metal coating. Prog Org Coat 71:110–116. https://doi.org/10.1016/j.porgcoat.2011.01.005
31. Chang CH, Huang TC, Peng CW et al (2012) Novel anticorrosion coatings prepared from polyaniline/graphene composites. Carbon 50:5044–5051. https://doi.org/10.1016/j.carbon.2012.06.043
32. Qing Y, Yang C, Yu N et al (2016) Superhydrophobic TiO_2/polyvinylidene fluoride composite surface with reversible wettability switching and corrosion resistance. Chem Eng J 290:37–44. https://doi.org/10.1016/j.cej.2016.01.013
33. Yeh TC, Huang TC, Huang HY et al (2012) Electrochemical investigations on anticorrosive and electrochromic properties of electroactive polyurea. Polym Chem 3:2209–2216. https://doi.org/10.1039/c2py20061a
34. Hosseini MG, Yardani P (2015) Electrochemical impedance spectroscopy evaluation on the anticorrosive performance of epoxy/polyaniline—ZnO nanocomposite coated mild steel under cathodic polarization. In: The 6th international color and coating congress electrochemical impedance spectroscope, pp 3–5

35. Xing C, Zhang Z, Yu L et al (2014) Anti-corrosion performance of nanostructured poly(aniline-co-metanilic acid) on carbon steel. Prog Org Coat 77:354–360. https://doi.org/10.1016/j.porgcoat.2013.10.010